Nonlinear response of global monsoon precipitation to Atlantic overturn-ing strength variations during Marine Isotope Stage 3

X. Zhang[1] , M. Prange[2], L.B. Ma[3], L. Jian[4]

[1]School of Atmospheric Sciences, Nanjing University of Information Science and Technology, Nanjing, China

[2] MARUM – Center for Marine Environmental Sciences, University of Bremen, Bremen, Germany

[3]The Institute of Atmospheric Physics, Chinese Academy of Sciences, Beijing, China

[4] School of Geography, Nanjing Normal University, Nanjing, China

Corresponding author: Xiao Zhang (xzhang@nuist.edu.cn)

Key Points:

- Nonlinear response of global monsoon rainfall to ocean circulation strength change in Marine Isotope Stage 3.
- Simulated rainfall change is consistant with reconstructed precipitation variation during millennial abrupt climate events.
- Nonlinearity in global monsoon rainfall is constrained by ocean heat transport.

Abstract

Monsoon rainfall proxy records show clear millennial variations corresponding to abrupt climate events in Greenland ice cores during Marine Isotope Stage 3 (MIS3). The occurrence of these abrupt climate changes is associated with Atlantic Meridional Overturning Circulation (AMOC) strength variations which greatly impact the global oceanic energy transport. Hence, the AMOC most likely plays a key role in modulating the global monsoon rainfall at millennial time scale. No modeling work has hitherto investigated the global monsoon system response to AMOC changes under a MIS3 background climate. Using a coupled climate model CCSM3, we simulated MIS3 climate using true 38 ka before present boundary conditions and performed a set of freshwater hosing/extraction experiments. We show not only agreement between modeling results and proxies of monsoon rainfall within global monsoon domain but also highlights a nonlinear relationship between AMOC strength and annual mean global monsoon precipitation related to oceanic heat transport constraints. During MIS3, a weakened AMOC could lead to an increase of annual mean global monsoon rainfall dominated by the southern hemisphere, whereas northern hemisphere monsoon rainfall decreases. Above about 16 Sverdrups a further strengthening of the AMOC has no significant impact on hemi-spheric and global monsoon domain annual mean rainfall. The seasonal monsoon rainfall showed same asymmetric response like annual mean both hemispherical and globally.

Plain Language Summary

1 Introduction

The concept of ‘global monsoon’ has been intensively studied during recent years either from a modern or paleoclimate perspective due to its great importance within the climate system and to human activities and livelihoods. From the paleoclimate community, different types of proxy records from various locations have been studied to examine monsoon rainfall variations over different time scales. Monsoon rainfall proxies have demonstrated millennial scale monsoon oscillations globally (Voelker, 2002; Cheng et al., 2012). Such millennial variation in precipitation could be forced by climate condition change in the North Atlantic that associated with observed abrupt climate shifts during the last glacial, namely, Dansgaard-Oeschger (D-O) events and ice melting events during Heinrich Stadials (HSs, Wang et al., 2001; Mohtadi & Prange, 2016). D-O events were featured with fast (within decades or less) shift from cold stadial to mild interstadial which lasts for several centuries in Greenland ice core. And they were especially pronounced during Marine Isotope Stage 3 (MIS3, approx. 57-29 ka years before present, Zhang & Prange, 2020). Heinrich Stadial 4 (HS4) occurred within MIS3 and was characterized by large iceberg-derived freshwater flux into the North Atlantic and a reduction of North Atlantic Deep Water (Elliot et al., 2001). The mechanisms behind millennial-scale monsoon variations and their linkage to high latitude forcing are still under debate and one potential candidate to explain such coupling processes is the Atlantic Meridional Overturning Circulation (AMOC, Sun et al., 2012), which is responsible for more than half of the global oceanic heat transport towards high northern latitudes (Ganachaud & Wunsch, 2000).

One robust but incomplete picture shown in proxy records is that NH summer monsoon was drier and SH summer monsoon was wetter during HSs and D-O cold phases (Want et al., 2008; Kenner et al., 2012). During D-O cold phases and HSs, the AMOC slowed down (Elliot et al., 2002). SST in the North Atlantic along with Greenland surface temperature dropped dramatically (Schulz, 2002) whereas the SH sur-face temperature increased (Voelker, 2002). Such so called bipolar seesaw pattern could substantially change meridional temperature gradients, transport the signal from the North Atlantic to the low latitudes, push the ITCZ into the SH (warmer hemisphere) and led to a drier Asian and North American summer monsoon and a wetter South American and Indo-Australian monsoon (Chiang & Friedman, 2012; Otto-Bliesner et al., 2014; Wen et al., 2016).

The AMOC is suggested to slow down in recent years (Praetorius, 2018) which might induce a bipolar seesaw and affect the monsoon rainfall. If this weaker AMOC continues to decrease in its strength, it might collapse and switch to an 'off' mode (Hofmann & Rahmstorf, 2009; Prange et al., 2003). However, the future of the AMOC is highly uncertain and an increase in its strength cannot be ruled out either (Bakker et al., 2016). The global monsoon system in a stronger than present day AMOC situation has seldom systematically analyzed although a persistently stronger AMOC could have existed during the last glacial cycle (Böhm et al., 2014). MIS3 serves as an ideal background climate to study the following questions due to its abrupt climate oscillations associated with AMOC strength variations: (1) How does the global monsoon rainfall response to AMOC strength variations associated with forcing from the high latitudes?

(2)Especially important, if the AMOC were to grow stronger, how would the global monsoon rainfall be affected?

2 Experiment design and Methods

The NCAR Community Climate System Model Version 3 (CCSM3, Collins et al., 2006; Yeager et al., 2006) is a full-complexity global general circulation model, which includes atmosphere, land, ocean and sea ice components. The atmosphere and land components share the T31 resolution in the horizontal (3.75°) and there are 26 vertical layers in the atmosphere and 10 soil layers in the land with activated dynamic vegetation module (Rachmayani et al., 2015). The ocean model has 25 vertical lev-els with layer thickness increasing from 8 m at the surface to around 500 m at the ocean bottom. The horizontal resolution is 3° at mid and high latitudes and around 0.9° around the equator with displaced North Pole over Greenland (Smith et al., 1995).

Using this model, we performed a 38 ka B.P. boundary condition control experiment, which represents the mid MIS3 period (referred as MIS3 in the manuscript), and 12 freshwater hosing/extraction experiments with freshwater perturbation in the Nordic Seas. The freshwater perturbation amount and experiment length are listed in Table S1. We use freshwater amount to refer to the specific sensitivity experiment, e.g. +0.2Sv test indicates we put 0.2Sv freshwater in the Nordic Seas whereas -0.2Sv means we extract 0.2Sv freshwater from the Nordic Sea surface. These model experiments apply different sea level and land-sea distribution, greenhouse gas con-centrations, orbital forcing and continental ice sheets compared to present day. All experiments were integrated long enough (> 500 years) to reach new equilibria, which has been tested by a student t-test (i.e. trend in the AMOC strength time series is not significant for the last 100 years of each simulation). The applied positive and negative freshwater perturbations ranged from ±0.005 Sv to ±0.2 Sv (1 Sv = 10^6 m3/s). All analyses in this study are based on the last 100 year average from each experiment.

3 Results and discussion

3.1 AMOC responses to external freshwater forcing

With positive freshwater forcing in the MIS3 North Atlantic, the strength of the AMOC decreased. A +0.2 Sv forcing is capable to cease the North Atlantic Deep Water Formation and the AMOC strength decreased from 15.38 Sv to 4.24 Sv. Same amount negative forcing (-0.2 Sv) had weaker impact on the AMOC strength. It resulted in an increase of the AMOC strength from 15.38 Sv to 21.45 Sv. Most importantly, a nonlinear response was seen in AMOC strength in response to freshwater flux (Fig. S1). We interpreted the weak AMOC state as cold stadials and strong circulation as mild interstadials in this study. Greenland surface temperature and NH winter sea ice cover also showed nonlinear shape as a function of freshwater perturbation (not shown here). Such abrupt change in temperature and ice cover was related to observed D-O events during MIS3 and ice melting events during HS4 (Zhang et al., 2014) and +0.2 Sv hosing experiment is interpreted as a simulation of HS4.

3.2 Model-proxy data comparison of global monsoon precipitation during MIS3

There are only a few rain-related proxy records spanning MIS3 allowing to reconstruct monsoon precipitation variability on millennial time scale. They all demonstrated a linkage between AMOC strength related abrupt climate shifts and monsoon precipitation. There are several records from South American sites at Botuvera (Wang et al., 2006; Wang et al., 2007), Peru (Cheng et al., 2013), Pacupahuain Cave (Kanner et al., 2012), Bahia State (Wang et al., 2004) and central eastern Brazil (Stríkis et al., 2018). All of these data showed a more humid South America when the NH was cooler connected to iceberg melting events in the North Atlantic during HSs.

Rainfall proxy from Hulu cave (Wang et al., 2001) and Songjia cave (Zhou et al., 2014) within the Asian monsoon region varied out-of-phase with records from South America above. A sharp increase in δ18O during HSs represented a weaker and drier east summer Asia monsoon during the NH cold phases. Meanwhile, two records from the Indian Monsoon region, Xiao Bailong Cave (Cai et al., 2006) and Arabia Sea sediment core SO130-289KL (Deplazes et al., 2016) indicated a weaker Indian Summer Monsoon during the cold stadials. Moreover, bulk Fe/K ratios from the north African monsoon region (core GeoB9508-5, Mulitza et al., 2008) correlating with oxygen isotope values in the NGRIP ice core(Andersen et al., 2004) showed arid conditions during the HSs, whereas higher Fe/K ratios in core CD154-17-17K indicated more humid south African conditions during the same intervals (Ziegler et al., 2013). Overall, millennial-scale resolution proxies in the two hemispheres varied anti-phased with each other in response to millennial-scale North Atlantic condition changes. An abrupt cooling in the North Atlantic surface corresponds to a weakening of NH summer monsoon and an intensified SH summer monsoon and vice versa. Such dipole pattern change in monsoon precipitation is associated with an AMOC-driven south-ward shift of the ITCZ and more asymmetric Hadley cells during the HSs. Most of the oxygen isotope records showed 2-3‰ differences comparing the cold HSs with warm interstadials, indicating a drop in seasonal precipitation in the NH and an increase in the SH. Xiao Bailong cave record experienced an especially strong change in the $\delta^{18}O$ signal, implying a significant weakening of the Indian Summer Monsoon when the AMOC was presumably weaker (Cai et al., 2015).

In our simulation results, for all records within the global monsoon region, model results are consistent with most of the observations, featuring enhanced SH summer monsoon rainfall and drier NH summer monsoon during the HSs. However, the model produced drier conditions during austral summer in western South America. Hence, at two sites (Pacupahuain cave and north Peru) the model showed less precipitation during HS4, which seems to contradict the proxy records. However, the reconstructed enhanced precipitation could also be related to austral winter precipi-tation, as previously been suggested (Campos et al., 2019). At the Hulu cave location, summer monsoon precipitation slightly increased during HS4 which is also incon-sistent with the proxy record. However, the simulated Pacific Subtropical High in HS4 is still weaker compared to the MIS3 control experiment. Last but not least, Indian Monsoon precipitation is largely reduced in the HS4 experiment.

3.3 Simulated global monsoon precipitation and wind responses to AMOC strength change

Freshwater forcing did not affect the AMOC strength symmetrically and both seasonal and annual global monsoon precipitation also show a nonlinear response to AMOC strength. Figure 1a shows annual mean precipitation in the MIS3 control run.

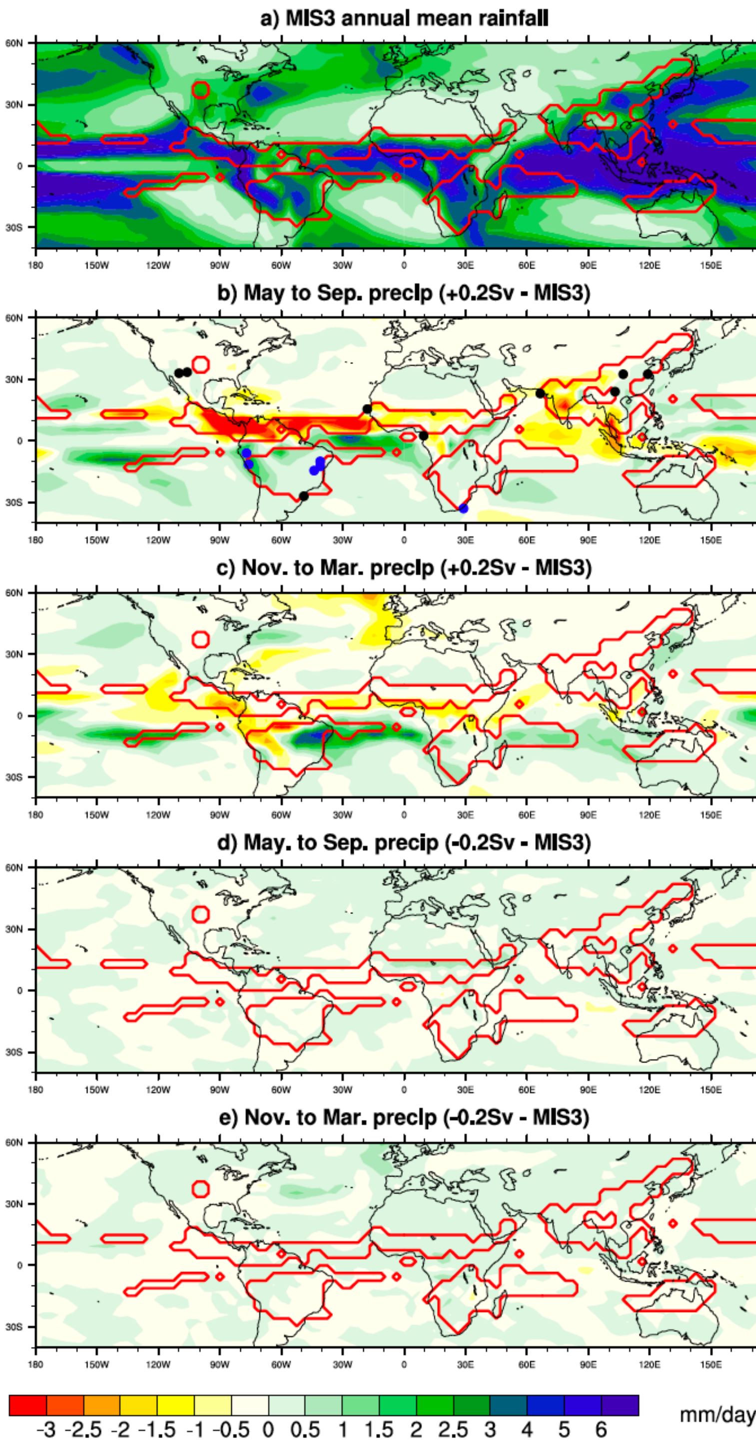

Figure 1. **Annual total precipitation and anomalies between different experiments.** a) MIS3 control run; b) difference between +0.2 Sv experiment and MIS3 control run during May to September; c) difference between +0.2 Sv experiment run and MIS3 control run during November to March; d) difference between -0.2 Sv experiment and MIS3 control run during May to September; and e) difference between -0.2 Sv experiment and MIS3 control run during November to March. Red contour area indicates the global monsoon region calculated by modeled rainfall data. Dots in **b** are the proxy record locations as it is discussed in section 3.4. Black indicates drier summer monsoon and blue indicates wetter summer monsoon.

The global monsoon domain (red contour) was defined using the following criteria (Wang et al., 2008; Wang et al., 2014): 1) annual mean local summer (May to Sep. in NH, Nov. to Mar. in SH) minus winter (May to Sep. in SH, Nov. to Mar. in NH) precipitation is greater than 300 mm and 2) local summer precipitation exceeds 55% of annual total rainfall. Compare to present day condition, the monsoon domain generally retreated in the north and expanded to the south over land compared due to decreased summer to annual precipitation ratio in a colder climate (Yan et al., 2016, Fig. 1a). We note however, that the global monsoon domain is not the focus of this study since the total area of global monsoon domain does not vary much over all model experiments.

The global monsoon region annual averaged rainfall rate is 3.43 mm/day in MIS3. When the AMOC decreased to 4.24 Sv during HS4 in the model, local summer mon-soon precipitation was generally reduced in the north and increased in the south. The strongest change in boreal summer monsoon precipitation was observed in tropical America and the tropical North Atlantic Ocean, featuring more than 3 mm/day precipitation decrease. The central equatorial Atlantic experiences maxi-mum rainfall increase, which is larger than 3 mm/day. The Asian-Australian mon-soon rainfall generally increases especially over east Asia (Fig. 1b). During boreal winter, the strongest rainfall change moves southward over the Pacific and the At-lantic associated with the seasonal shift of the Intertropical Convergence Zone. Moreover, a strong rainfall increase is simulated over Northeast Brazil (Fig. 1c).

In the case that AMOC strength increased to 21.45 Sv in the -0.2Sv experiment, the monsoon precipitation responded generally oppositely and about one order of magnitude weaker compared to the +0.2 Sv run in boreal winter and summer. The most significant increase in rainfall was observed in the African monsoon region (Figure 1d and 1e).

The statistical significance (at 95% confidence level) of the surface temperature differences between the ±0.2 Sv runs and the MIS3 control run, calculated using a student t-test, is shown in Figure 2. The same test is applied for surface wind differences. In the +0.2 Sv experiment, during May to September, Northern Indian Ocean surface temperature slightly decreased and continental surface temperature increased, which resulted in a stronger meridional temperature gradient and westerly wind anomalies, thus strengthening regional summer monsoon wind. Weaker monsoon winds were observed over East Asia and western Africa associated with weaker land-ocean temperature contrasts compared to the unperturbed MIS3 control run. The wind anomalies blew towards the Australian continent, indicating a weaker winter monsoon surface flow (Fig. 2a). As for November to March, wind anomalies were directed away from the continent in the East Asian and African monsoon regions whereas over Australia, a northwest wind anomaly was seen. However, temperature and wind changes in northern Australia were not significant (Fig. 2b). Generally speaking, when the AMOC became weaker with positive fresh-water forcing, during boreal summer, the global monsoon reduced its wind strength whereas during boreal winter, the global monsoon surface flow became stronger.

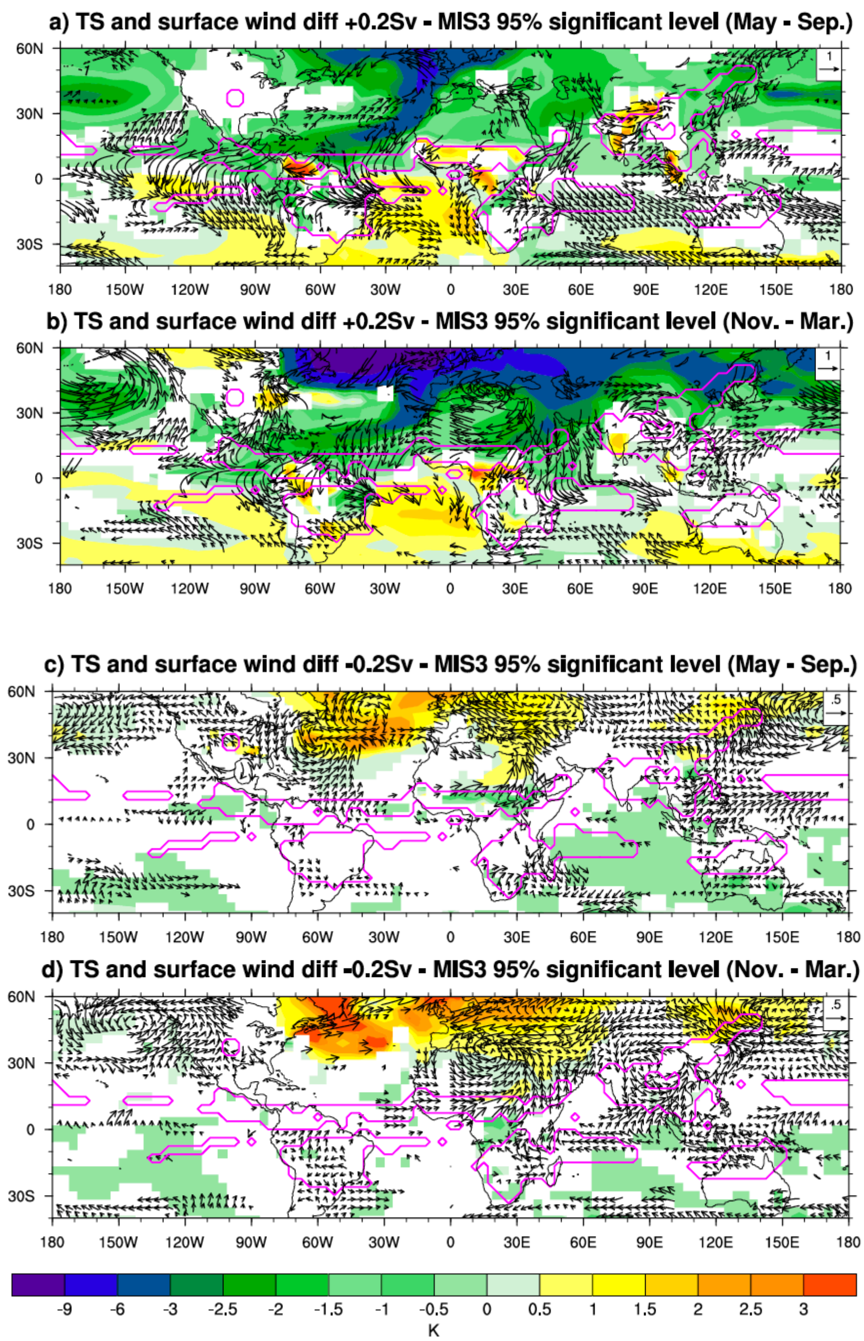

Figure 2. **Surface wind and surface temperature differences.** a) May to September difference between +0.2 Sv experiment and MIS3 control run; b) November to March difference between +0.2 Sv experiment and MIS3 control run and; c) same as panel **a** but for the -0.2 Sv experiment; and d) same as panel **b** for the -0.2 Sv experiment. Wind difference vector unit: meter per second. Values above 95% confidence level are shown. Pink contour area indicates the global monsoon region as the same in figure 1.

For an AMOC stronger than the MIS3 baseline state with saltier North Atlantic surface water due to freshwater extraction, simulated winds and temperatures showed changes in opposite direction. Global monsoon flow became stronger in boreal summer and weaker in boreal winter. However, with the same magnitude of freshwater perturbation (-0.2 Sv), the monsoon responses were much weaker. Between May and September, most of the SH ocean experienced a cooling of less than 1 degree and NH warming was generally seen only above 20°N with maximum of around 3 degrees in the central North Atlantic. Surface wind change was less than 1 m/s and generally in opposite direction compared to the +0.2 Sv experiment (Fig. 2c). During November to March, NH warming was slightly stronger than in boreal summer in mid and high latitudes over the North Atlantic and surface wind change had a similar pattern as during May to September in the monsoon regions (Fig. 2d).

The annual mean precipitation in the global monsoon domain increased rather linearly when the AMOC strength was below 15.38 Sv with positive freshwater hosing but kept at a steady level at around 3.4 mm/day when we imposed negative forcing in the Nordic Seas (Fig. 3a). The mean ITCZ latitude (defined as the median latitude of maximum annual mean precipitation between 20°N and 20°S) moves southward with decreasing AMOC strength. The mean ITCZ location was constantly around 0.3°N when the AMOC increased from 15.38 Sv to 21.45 Sv, but it moved southward and even reached the SH when the AMOC strength decreased to 4.24 Sv. Separating local summer and winter precipitation in the NH and SH gave a quite similar figure. In both hemispheres, local summer and winter monsoon precipitation no longer sig-nificantly increases or decreases when the AMOC reaches ca. 16 Sv. However, in both seasons, monsoon precipitation decreased linearly in the north and increased in the south when the AMOC strength decreased with positive freshwater forcing (Fig. 3b and 3c). The SH monsoon rainfall dominated the annual mean global monsoon rainfall since the ITCZ moved southward when the AMOC weakened.

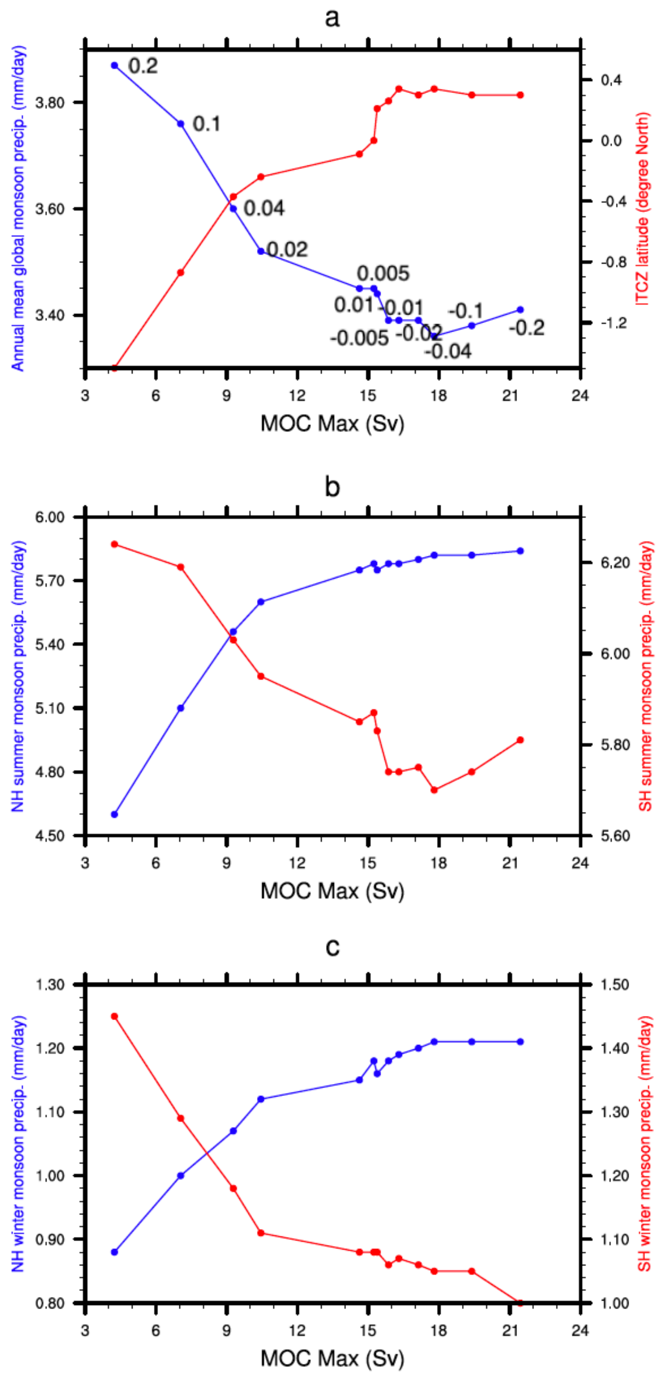

Figure 3. **Climate responses to AMOC strength change.** a) Mean ITCZ position and average annual precipitation rate in global monsoon region as indicated in Figure 2 as a function of AMOC strength; b) average summer (May to September for NH and November to March for SH) precipitation rate in global monsoon region as a function of AMOC strength in the two hemispheres; and c) same as b but for hemispheric winter (November to March for NH and May to September for SH).

3.4 Mechanism of global monsoon precipitation change as response to AMOC strength variation

The monsoon-ocean coupled system is influenced by tropical SSTs and the polar ice sheets (Webster et al., 1994; Pierrehumbert, 2000). The AMOC can affect both by redistributing ocean heat content. Meanwhile, a weaker AMOC, less northward oceanic heat transport, larger sea ice cover and colder surface temperature in Greenland is associated with D-O cold phases and vice versa. D-O event signals could be found in the tropics over the monsoon region (Zhang et al., 2015). The spread of their impact from the high latitudes to the tropics due to AMOC strength variations could be a plausible explanation of millennial scale global monsoon variability as it is observed in the proxy records.

The high-low latitude teleconnection of global monsoon response to D-O type climate oscillations through AMOC strength variations is clearly seen in our simulated results. Taking the +0.2 Sv freshwater hosing experiment as an example, the AMOC strength significantly decreased as proxy records have shown that melted ice has greatly reduced North Atlantic Deep Water Formation during HS4. North Atlantic surface temperatures dropped by more than 20 degrees at high latitudes since the freshwater decreased ocean shallow layer salinity and hampered convection. A bipolar seesaw pattern was shown due to less oceanic heat transport to the north (Stocker et al., 2003) and amplifying feedbacks like a higher albedo. Temperature seesaw also led to a specific humidity seesaw in the model. There was less atmos-pheric water vapor in the north, while the SH became wetter. What is more, in our simulations, the NH ice cover expanded due to low temperature and directly affect-ed the atmospheric circulation pattern in the high and mid-latitudes. Coupling of the ocean and the atmosphere brought this impact to the low latitudes through stronger northward atmospheric heat transport (Fig. 4)

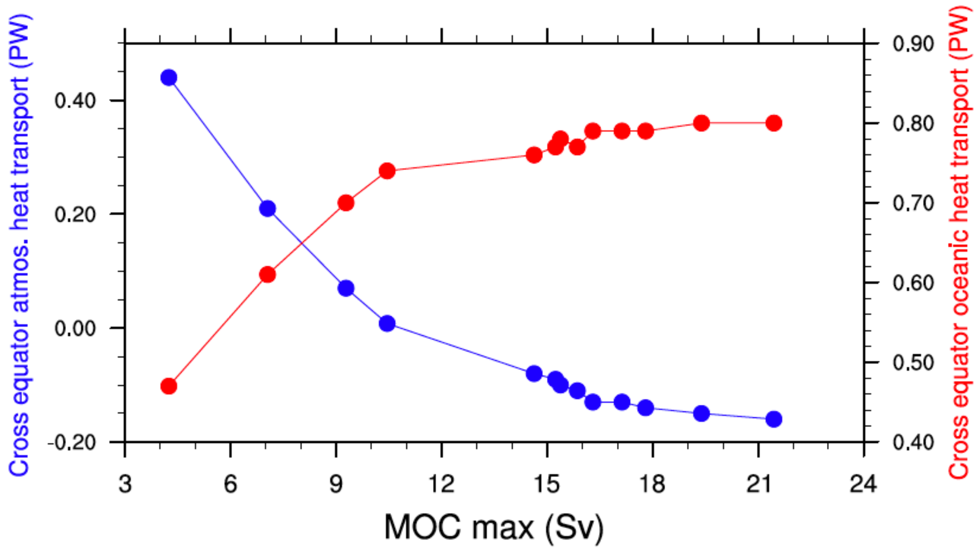

Figure 4. **Cross equatorial oceanic and atmospheric heat transports as a function of AMOC strength.**

and promoted a southward shift of the ITCZ (Chiang et al., 2003; Zhang & Delworth, 2005; Frierson et al., 2013, Fig. 3a). Corresponding to the southward shift of ITCZ, the tropical meridional SST gradient became sharper between the two hemispheres (Fig. 5). Our simulated ITCZ latitude shift in response to cross equatorial atmospheric heat transport change is about

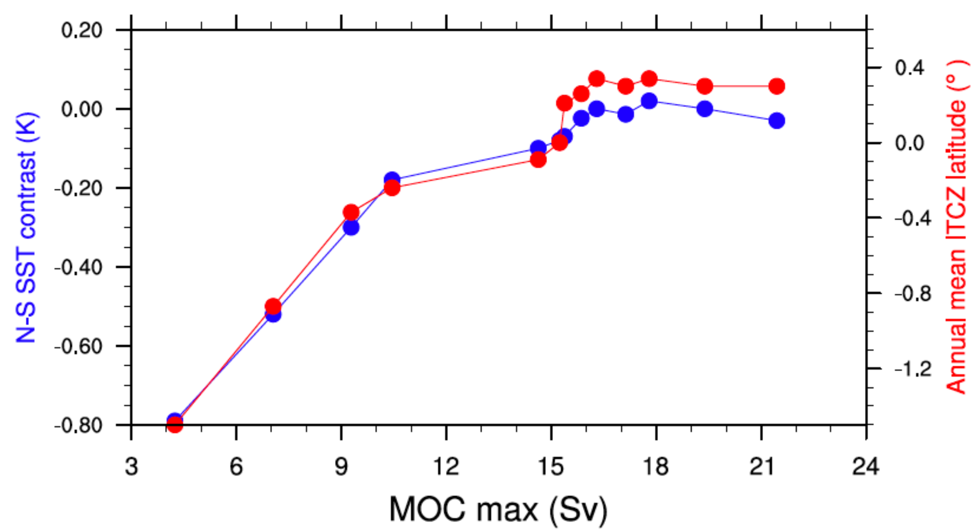

Figure 5. **North-South SST contrast and mean ITCZ latitude as a function of AMOC strength.** North-South SST contrast is defined as the annual mean SST difference between 20°N to the equator and 20°S to the equator.

-3° /PW, which is comparable to the PMIP2 Last Glacial Maximum ensemble mean (Donohoe et al., 2013). The seasonal cycle of ITCZ latitude as function of cross equatorial atmospheric heat transport and meridional SST contrast also matches the CMIP3 ensemble mean (McGee et al., 2014). Apart from a latitudinal shift to the warmer hemisphere of its rising branch, the Hadley cell also became weaker in the SH and stronger in the NH during boreal summer and winter which was due to reduced oceanic heat transport as well (Fig. 6a and 6c).

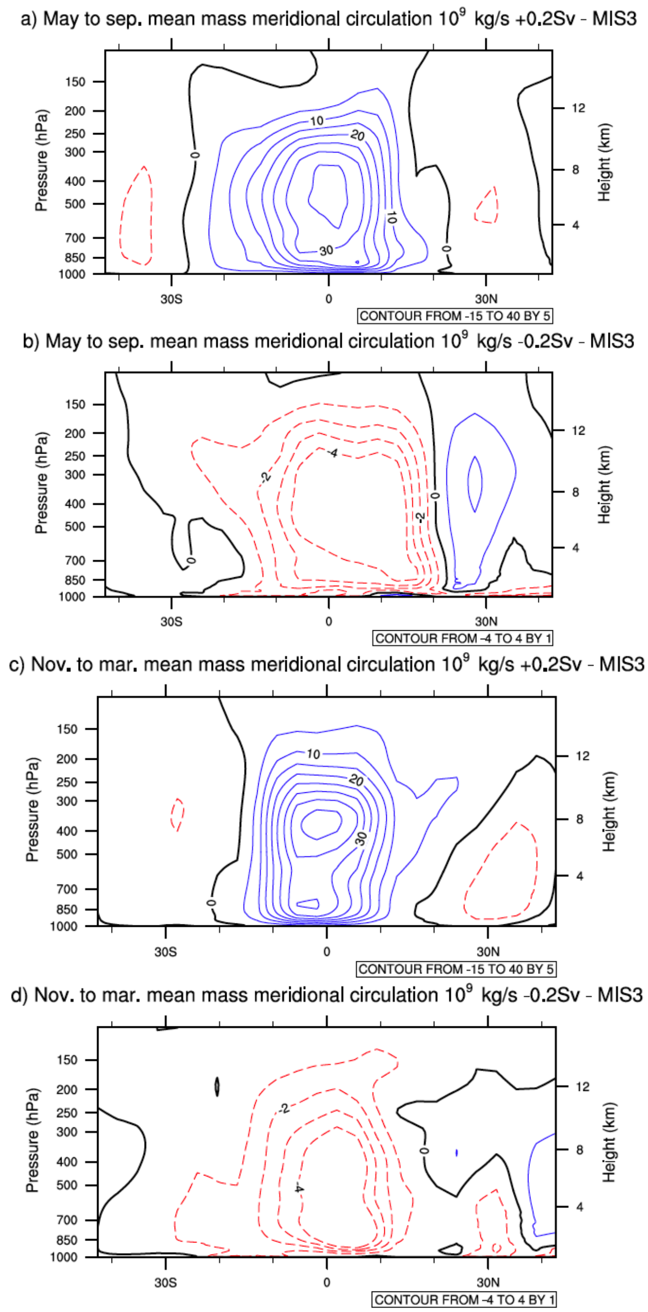

Figure 6. **Mean meridional mass streamfunction differences.** a) +0.2 Sv–MIS3 control run (May to September); b) -0.2 Sv–MIS3 control run (May to September); c) same as a but for November to March; and d) same as b but for November to March. Positive values indicate clockwise circulation and negative values indicate counterclockwise circulation.

A colder NH generally led to stronger subsidence and less atmospheric water vapor content. A warmer SH favored uplifting of moist air and higher specific humidity compared to MIS3 baseline conditions. As a consequence, the NH summer monsoon rainfall was reduced, while SH and global monsoon rainfall increased. The above process grew stronger when we put more freshwater into the North Atlantic as it is shown in Figure 3. The oppo-site (D-O warm phase) is true for a stronger AMOC when we extract freshwater in the North Atlantic. The NH became warmer and wetter which led to more monsoon rainfall. The SH became cooler, drier and the monsoon rainfall was reduced. The SH Hadley cell was strengthened, while the NH Hadley cell was weakened (Fig. 6b and 6d). The ITCZ moved northward and the annual mean rainfall within global monsoon domain decreased. However, same amounts of freshwater extraction resulted in much weaker responses compared to freshwater injection as it is shown in Figure 3. The annual mean rainfall in global monsoon domain did not further increase and the ITCZ stayed around 0.4°N when the AMOC strength reached ca. 16 Sv and above. The asymmetrical monsoon precipitation response is related to a nonlinearity in oceanic and atmospheric heat transport. Oceanic and atmospheric cross equatorial heat transports responded linearly to positive freshwater injections but did not vary much when the perturbations were negative. When the AMOC slowed down with a +0.2 Sv freshwater injection, cross equatorial ocean heat transport decreased from 0.8 PW to less than 0.5 PW. To compensate such energy transport change, the atmos-phere carried approximately 0.4 PW heat from the SH to the NH (Fig. 4).

To further investigate monsoon rainfall and circulation changes in individual mon-soon domain, 1000-500 hPa water vapor flux along with 500hPa vertical velocity in the ±0.2 Sv experiments was compared with MIS3 control run. MIS3 control experiment showed strong water vapor convergence towards individual local summer monsoon domain accompanied with upward motion (Fig 7a and 7b). In the +0.2 Sv case during boreal summer, water vapor was transported away from Asian and African monsoon regions accompanied with weaker upward motion (except eastern part of Asia) whereas in the SH, water vapor was transported towards the monsoon region and vertical motion was strengthened (Fig. 7c). In boreal winter, though ver-tical motion increased over India, large parts of Asia experience anomalous subsidence. In the

SH, stronger vertical motion and enhanced water vapor transport were simulated in the monsoon region (Fig. 7d). In general, the NH monsoon rainfall de-creased and the SH

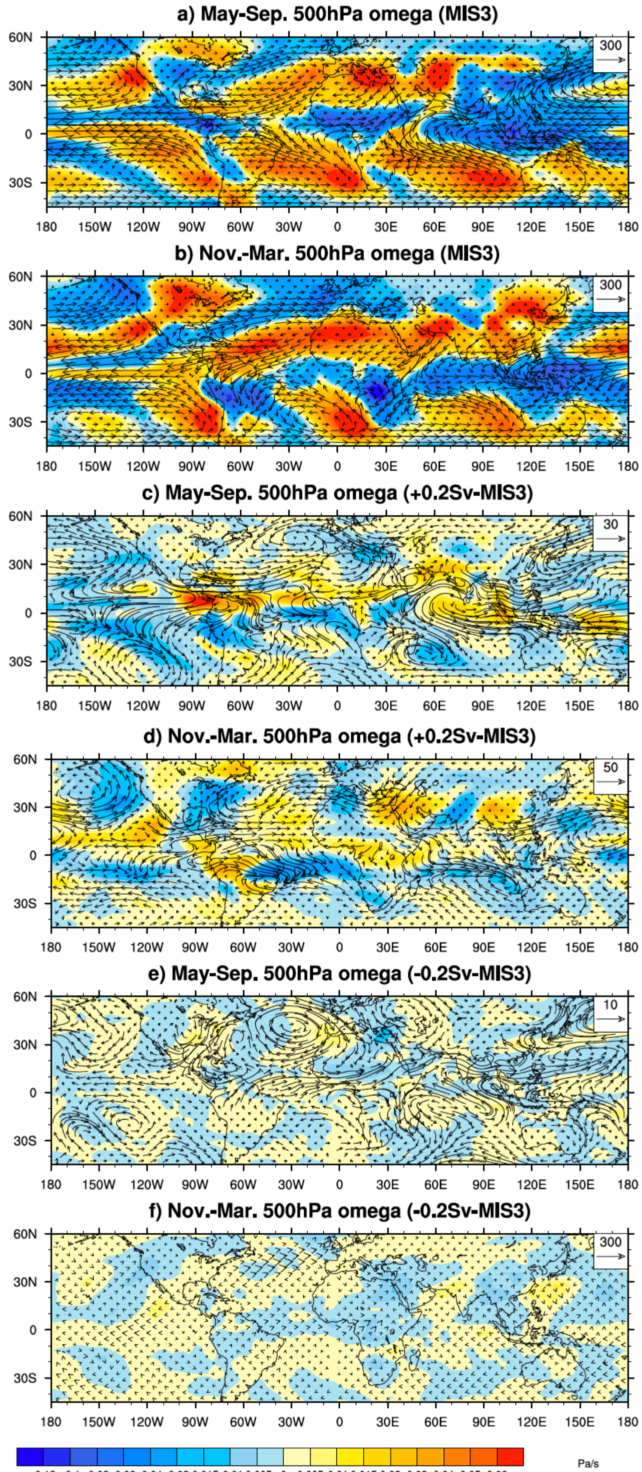

Figure 7. **1000-500 hPa water vapor flux and 500 hPa omega (vertical pressure velocity).** a) May to September mean in MIS3 control run; b) November to March mean in MIS3 control run; c) May to September difference between

+0.2 Sv experiment and MIS3 control run; d) same as a but for November to March; e) same as a but for the -0.2 Sv experiment; and f) same as b but for the -0.2 Sv experiment. Vector unit: kg/m/s, omega unit: Pa/s.

experienced more monsoon rainfall in both seasons. The -0.2 Sv case showed different and weaker responses. In both seasons, the NH experienced stronger upward motion at 500hPa level in East Asian and African monsoon region and water vapor converged towards monsoon regions whereas in the SH water va-por was mostly transported away from the monsoon regions accompanied with weaker vertical motion (Fig. 7e and 7f).

Overall, based on our results, the AMOC strength showed a strong nonlinear behavior to freshwater perturbation and AMOC strength variations induced nonlinear responses in surface conditions including monsoon precipitation (annually and season-ally) corresponding to cold stadial and warm interstadial conditions.

4 Conclusions

This study provides an integrated picture of global monsoon rainfall changes between cold stadials and mild interstadials during MIS3 by combining modeling re-sults and proxies. The modeled monsoon rainfall variations are mostly consistent with proxy records. Such agreement provides further confidence in model simula-tions of global monsoon changes under climates different from the modern one and may aid the current monsoon research. The global monsoon precipitation response to AMOC strength changes under MIS3 background climate was analyzed in detail and it was found that total annual and seasonal rainfall within the global monsoon region show a nonlinear response to freshwater-induced AMOC changes. Corresponding to D-O cold phases (stadials), positive freshwater perturbations in the Nordic Seas slowed down the AMOC, decreased northward ocean heat transport, hence, cooled the NH and warmed the SH, which led to a more southward posi-tioned ITCZ along with a more asymmetrical Hadley cell and an increase in annual global monsoon precipitation in the south and a decrease of monsoon rainfall in the north. A more vigorous circulation induced by freshwater extraction did not have significant impact on monsoon rainfall globally and in the two hemispheres individually since the oceanic heat transport was hardly affected. The bipolar seesaw pat-tern was much less significant, meridional SST contrast in the tropics limited and the ITCZ position stayed stable. As a result, the main factor affecting monsoon pre-cipitation in the model is the oceanic heat transport associated with the AMOC be-tween the hemispheres.

Combining both model data and paleo records, our work showed a clear picture of global monsoon precipitation response to high latitude climate variations tied to abrupt climate oscillations during MIS3, which provides insight into high-low latitude teleconnections for both present and past climates.

Acknowledgments

Model simulations in this study were carried out at Der Norddeutsche Verbund für Hoch- und Höchstleistungsrechnen (HLRN) and supported by the National Natural Science Foundation of China (project number: 2081011619301), the PalMod project funded by the German Federal Ministry of Education and Science (BMBF), and the DFG Research Center/Cluster of Excellence "The Ocean in the Earth System".

The authors whose names are listed certify that they have NO affiliations with or involvement in any organization or entity with any financial interest in the subject matter or materials discussed in this manuscript.

References

1. Voelker, A.H.L. (2002). Global distribution of centennial-scale records for Marine Isotope Stage (MIS) 3: a database. *Quat. Sci. Rev., 21,* 1185–212.
2. Cheng, H. et al. (2012). The Global Paleomonsoon as seen through speleothem records from Asia and the Americas. *Clim. Dyn., 39,* 1045-1062.
3. Wang, Y.J. et al. (2001). A high-resolution absolute-dated Late Pleistocene monsoon record from Hulu Cave, China. *Science, 294,* 2345–2348.
4. Mohtadi, M., Prange, M., and Steinke, S. (2016). Palaeoclimatic insights into forcing and response of monsoon rainfall. *Nature, 533,* 191-199, doi:10.1038/nature17450.
5. Zhang, X., & Prange, M. (2020). Stability of the Atlantic overturning circulation under intermediate (MIS3) and full glacial (LGM) conditions and its relationship with Dansgaard-Oeschger climate variability. *Quat. Sci. Rev., 242,* 106443.
6. Elliot, M. et al. (2001). Coherent patterns of ice-rafted debris deposits in the Nordic regions during the last glacial (10-60 ka). *Earth Planet. Sci. Lett., 194,* 151-163.
7. Sun, Y.B. et al. (2012). Influence of Atlantic meridional overturning circulation on the East Asian winter monsoon. *Nat. Geosci., 5,* 46–49.
8. Ganachaud, A. & Wunsch, C. (2000). Improved estimates of global ocean circulation, heat transport and mixing from hydrographic data. *Nature, 408(6811),* 453–457.
9. Wang, Y.J. et al. (2008). Millennial- and orbital-scale changes in the East Asian monsoon over the past 224,000 years. *Nature, 28,* 1090–1093.
10. Kanner, L. C., Burns, S. J., Cheng, H., and Edwards, R. L. (2012). High latitude forcing of the South American summer monsoon during the last glacial. *Science, 335,* 570–573.
11. Elliot et al. (2002). Changes in North Atlantic deep-water formation associated with the Dansgaard–Oeschger temperature oscillations (60–10 ka). *Quat. Sci. Rev., 21,* 1153-1165.
12. Schulz, M. (2002). On the 1470-year pacing of Dansgaard-Oeschger warm events. *Paleoceanography, 17(2),* doi:10.1029/2000PA000571.
13. Chiang, J.C.H. & Friedman, A.R. (2012). Extratropical cooling, interhemispheric thermal gradients, and tropical climate change. *Annu. Rev. Earth Planet. Sci., 40,* 383-412.

14. Otto-Bliesner, B.L. et al. (2014). Coherent changes of southeastern equatorial and northern African rainfall during the last deglaciation. Science, 346,1223-1227.
15. Wen, X., Liu, Z., Wang, S., Cheng, J., Zhu, J. (2016). Correlation and anti-correlation of the East Asian Summer and Winter Monsoons during the last 21,000 years. *Nat. Commun., 7,* 11999.
16. Praetorius, S. K. (2018). North Atlantic circulation slows down. *Nature, 556,* 180-181, doi:10.1038/s41586-018-0006-5.
17. Hofmann, M. & Rahmstorf, S. (2009). On the stability of the Atlantic meridional overturning circulation. *Proc. Natl. Acad. Sci. U.S.A., 106,* 20584–20589.
18. Prange, M., Lohmann, G. and Paul, A. (2003). Influence of vertical mixing on the thermohaline hysteresis: Analyses of an OGCM. *Journal of Physical Oceanography, 33(8),* 1707-1721.
19. Bakker, P., et al. (2016). Fate of the Atlantic Meridional Overturning Circulation: Strong decline under continued warming and Greenland melting. *Geophys. Res. Lett., 43,* 12252–12260, doi:10.1002/2016GL070457.
20. Böhm, E. et al. (2014). Strong and deep Atlantic Meridional Overturning Circulation during the last glacial cycle. *Nature, 517,* 73-76.
21. Collins, D.W. et al. (2006). The Community Climate System Model Version 3 (CCSM3). *J. Clim., 19,* 2122–2143.
22. Yeager, S.G. et al. (2006). The low-resolution CCSM3. *J. Clim., 19,* 2545–2566.
23. Rachmayani, R., Prange, M, and Schulz, M. (2015). North African vegetation-precipitation feedback in early and mid-Holocene climate simulations with CCSM3-DGVM. *Climate of the Past, 11,* 175-185, doi:10.5194/cp-11-175-2015.
24. Smith, R. D., Kortas, S. & Meltz, B. (1995). Curvilinear coordinates for global ocean models. Tech. Rep. LA-UR-95-1146, Los Alamos National Laboratory, 50 pp.
25. Zhang, X., Prange, M., Merkel, U. & Schulz, M. (2014). Instability of the Atlantic overturning circulation during Marine Isotope Stage 3. *Geophys. Res. Lett., 41,* 4285-4293.
26. Wang, X. et al. (2006). Interhemispheric anti-phasing of rainfall during the last glacial period. *Quat. Sci. Rev., 25,* 3391–3403.
27. Wang, X. et al. (2007). Millennial-scale precipitation changes in southern Brazil over the past 90 000 years. Geophys. Res. Lett., 34, L23701,doi:10.1029/2007GL031149.
28. Cheng, H. et al. (2013). Climate change patterns in Amazonia and biodiversity. *Nature Commun., 4,* 1411, doi:10.1038/ncomms2415.
29. Wang, X., Auler, A., Edwards, R. et al. (2004). Wet periods in northeastern Brazil over the past 210 kyr linked to distant climate anomalies. *Nature, 432,* 740–743.
30. Stríkis, et al. (2018). South American monsoon response to iceberg discharge in the North Atlantic. *Proc. Natl. Acad. Sci. U.S.A., 115 (15),* 3788-3793.
31. Zhou et al. (2014). Heinrich event 4 and Dansgaard/Oeschger events 5–10 recorded by high-resolution speleothem oxygen isotope data from central China, *Quat. Res., 82,* 394-404.
32. Cai, Y.J. et al. (2006). High-resolution absolute-dated Indian Monsoon record between 53 and 36 ka from Xiaobailong Cave, southwestern China. *Geology, 34,* 621–624.
33. Deplazes, G. et al. (2016). Links between tropical rainfall and North Atlantic climate during the last glacial period. *Nat. Geosci., 6,* 213–217. doi:10.1038/NGEO1712.
34. Mulitza, S. et al. (2008). Sahel megadroughts triggered by glacial slowdowns of Atlantic meridional overturning. *Paleoceanography, 23,* PA4206.
35. Andersen et al. (2004). High-resolution record of Northern Hemisphere climate extending into the last interglacial period. Nature, 431(7005), 147-151.

36. Ziegler, M. et al. (2013). Development of Middle Stone Age innovation linked to rapid climate change. *Nat. Commun., 4,* 1905.
37. Cai, Y.J. et al. (2015). Variability of stalagmite-inferred Indian monsoon precipitation over the past 252,000 y. *Proc. Natl. Acad. Sci. U. S. A., 112(10),* 2954–2959.
38. Campos et al. (2019). A new mechanism for millennial scale positive precipitation anomalies over tropical South America. *Quat. Sc. Rev., 225,* 105990.
39. Wang, B. & Ding, Q. (2008). Global monsoon: Dominant mode of annual variation in the tropics. *Dynam. Atmos. Oceans, 44(3/4),* 165-183.
40. Wang et al. (2014). The global monsoon across timescales: coherent variability of regional monsoons, *Clim. Past, 10,* 2007–2052, https://doi.org/10.5194/cp-10-2007-2014.
41. Yan, M., Wang, B. & Liu, J. (2016). Global monsoon change during the Last Glacial Maximum: a multi-model study. *Clim. Dyn., 47,* 359–374.
42. Webster, P.J. (1994). The role of hydrological processes in ocean-atmosphere interactions. Rev. *Geophys., 32,* 427–476.
43. Pierrehumbert, R.T. (2000). Climate change and the tropical Pacific: the sleeping dragon wakes. Proc. Natl. Acad. Sci. U. S. A., 97, 1355–1358.
44. Zhang, X., Prange, M., Merkel, U., & Schulz, M. (2015). Spatial fingerprint and magnitude of changes in the Atlantic meridional overturning circulation during Marine Isotope Stage 3. *Geophys. Res. Lett., 42,* 1903-1911.
45. Stocker, T. F. & Johnsen, S. J. (2003). A minimum thermodynamic model for the bipolar seesaw. *Paleoceanography, 18(4),* 1087.
46. Chiang, J., Biasutti, M., and Battisti, D. (2003). Sensitivity of the Atlantic Intertropical Convergence Zone to Last Glacial Maximum boundary conditions. *Paleoceanography., 18,* 1094.
47. Zhang, R., and Delworth, T. (2005). Simulated Tropical Response to a Substantial Weakening of the Atlantic Thermohaline Circulation. *J. Clim., 18,* 1853-1860.
48. Frierson, D. M. W. et al. (2013). Contribution of ocean overturning circulation to tropical rainfall peak in the Northern Hemisphere. *Nat. Geosci., 6(11),* 940–944 doi:10.1038/ngeo1987.
49. Donohoe, A., Marshall, J., Ferreira, D. & McGee, D. (2013). The relationship between ITCZ location and cross-equatorial atmospheric heat transport: from the seasonal cycle to the last glacial maximum. *J. Clim., 26,* 3597–3618.
50. McGee, D., Donohoe, A., Marshall, J., & Ferreira, D. (2014). Changes in ITCZ location and cross-equatorial heat transport at the Last Glacial Maximum, Heinrich Stadial 1, and the mid-Holocene. *Earth Planet. Sci. Lett., 390,* 69–79.